

# Chiral effective field theory on the lattice at next-to-leading order

Buğra Borasoy<sup>a</sup>, Evgeny Epelbaum<sup>b,a</sup>, Hermann Krebs<sup>a,b</sup>, Dean Lee<sup>c,a</sup>, Ulf-G. Meißner<sup>a,b</sup>

<sup>a</sup>*Helmholtz-Institut für Strahlen- und Kernphysik (Theorie) Universität Bonn,  
Nußallee 14-16, D-53115 Bonn, Germany*

<sup>b</sup>*Institut für Kernphysik (Theorie), Forschungszentrum Jülich, D-52425 Jülich, Germany*

<sup>c</sup>*Department of Physics, North Carolina State University, Raleigh, NC 27695, USA*

## Abstract

We study nucleon-nucleon scattering on the lattice at next-to-leading order in chiral effective field theory. We determine phase shifts and mixing angles from the properties of two-nucleon standing waves induced by a hard spherical wall in the center-of-mass frame. At fixed lattice spacing we test model independence of the low-energy effective theory by computing next-to-leading-order corrections for two different leading-order lattice actions. The first leading-order action includes instantaneous one-pion exchange and same-site contact interactions. The second leading-order action includes instantaneous one-pion exchange and Gaussian-smearred interactions. We find that in each case the results at next-to-leading order are accurate up to corrections expected at higher order.

## I. INTRODUCTION

There have been several recent studies on the subject of lattice simulations for low-energy nuclear physics using effective interactions [1, 2, 3, 4, 5, 6, 7, 8, 9, 10, 11, 12, 13, 14, 15, 16]. Here we present a study of nucleon-nucleon scattering on the lattice at next-to-leading order in chiral effective field theory for momenta less than or equal to the pion mass. This analysis is part of a long-term effort to put the formalism of chiral effective field theory on the lattice and use the lattice action to study few- and many-nucleon systems. This is the first of a pair of papers on lattice chiral effective field theory at next-to-leading order. In this first paper we calculate lattice phase shifts and mixing angles and fit unknown operator coefficients at next-to-leading order using the spherical wall method introduced in [17]. In the companion paper we use the resulting lattice action to perform Monte Carlo simulations of dilute neutron matter.

The organization of this paper is as follows. We begin with a review of the effective potential for chiral effective field theory at next-to-leading order and simplifications which can be made at low cutoff momentum. We then discuss a general test of model independence at fixed lattice spacing. We illustrate this model independence explicitly by repeating all calculations using two different lattice actions. The first action uses instantaneous one-pion exchange and same-site contact interactions at leading order. The second leading-order action includes instantaneous one-pion exchange and Gaussian-smearred interactions. Both of these lattice actions were first introduced in [13]. We compute next-to-leading-order corrections for these actions and find results accurate up to omitted higher-order terms.

## II. CHIRAL EFFECTIVE FIELD THEORY AT NEXT-TO-LEADING ORDER

### A. Effective potential

In the following  $\vec{q}$  denotes the  $t$ -channel momentum transfer for nucleon-nucleon scattering while  $\vec{k}$  is the  $u$ -channel exchanged momentum transfer. At leading order (LO) in the Weinberg power-counting scheme [18, 19] the  $NN$  effective potential consists of two independent contact terms and instantaneous one-pion exchange (OPEP),

$$V_{\text{LO}} = V^{(0)} + V^{\text{OPEP}}, \quad (1)$$

$$V^{(0)} = C_S + C_T (\vec{\sigma}_1 \cdot \vec{\sigma}_2), \quad (2)$$

$$V^{\text{OPEP}} = - \left( \frac{g_A}{2f_\pi} \right)^2 \boldsymbol{\tau}_1 \cdot \boldsymbol{\tau}_2 \frac{(\vec{\sigma}_1 \cdot \vec{q})(\vec{\sigma}_2 \cdot \vec{q})}{q^2 + m_\pi^2}. \quad (3)$$

The vector arrow in  $\vec{\sigma}$  signifies the three-vector index for spin. The boldface for  $\boldsymbol{\tau}$  signifies the three-vector index for isospin. We take for our physical constants  $m = 938.92$  MeV as the nucleon mass,  $m_\pi = 138.08$  MeV as the pion mass,  $f_\pi = 93$  MeV as the pion decay constant, and  $g_A = 1.26$  as the nucleon axial charge.

At next-to-leading order (NLO) the effective potential introduces seven independent contact terms carrying two powers of momentum, corrections to the two LO contact terms, and instantaneous two-pion exchange (TPEP) [20, 21, 22, 23, 24]. Using the notational conventions of [23, 24] we have

$$V_{\text{NLO}} = V_{\text{LO}} + \Delta V^{(0)} + V^{(2)} + V_{\text{NLO}}^{\text{TPEP}}. \quad (4)$$

The contact interactions are given by

$$\Delta V^{(0)} = \Delta C_S + \Delta C_T (\vec{\sigma}_1 \cdot \vec{\sigma}_2), \quad (5)$$

$$\begin{aligned} V^{(2)} = & C_1 q^2 + C_2 k^2 + (C_3 q^2 + C_4 k^2) (\vec{\sigma}_1 \cdot \vec{\sigma}_2) + i C_5 \frac{1}{2} (\vec{\sigma}_1 + \vec{\sigma}_2) \cdot (\vec{q} \times \vec{k}) \\ & + C_6 (\vec{\sigma}_1 \cdot \vec{q})(\vec{\sigma}_2 \cdot \vec{q}) + C_7 (\vec{\sigma}_1 \cdot \vec{k})(\vec{\sigma}_2 \cdot \vec{k}), \end{aligned} \quad (6)$$

and the NLO two-pion exchange potential is [25, 26]

$$\begin{aligned} V_{\text{NLO}}^{\text{TPEP}} = & - \frac{\boldsymbol{\tau}_1 \cdot \boldsymbol{\tau}_2}{384\pi^2 f_\pi^4} L(q) \left[ 4m_\pi^2 (5g_A^4 - 4g_A^2 - 1) + q^2 (23g_A^4 - 10g_A^2 - 1) + \frac{48g_A^4 m_\pi^4}{4m_\pi^2 + q^2} \right] \\ & - \frac{3g_A^4}{64\pi^2 f_\pi^4} L(q) [(\vec{q} \cdot \vec{\sigma}_1)(\vec{q} \cdot \vec{\sigma}_2) - q^2 (\vec{\sigma}_1 \cdot \vec{\sigma}_2)], \end{aligned} \quad (7)$$

where

$$L(q) = \frac{1}{2q} \sqrt{4m_\pi^2 + q^2} \ln \frac{\sqrt{4m_\pi^2 + q^2} + q}{\sqrt{4m_\pi^2 + q^2} - q}. \quad (8)$$

## B. Simplified form at low cutoff

In this paper we consider low-energy nucleon-nucleon scattering at momenta less than or equal to the pion mass,  $m_\pi$ . On the lattice the ultraviolet cutoff momentum,  $\Lambda$ , equals  $\pi$  divided by the lattice spacing,  $a$ . If we focus narrowly on calculations of two-nucleon scattering

on the lattice we can take any sufficiently small lattice spacing satisfying  $\Lambda \gg m_\pi$ . However serious numerical difficulties appear at large  $\Lambda$  in Monte Carlo simulations of few- and many-nucleon systems. In some attractive channels we might find spurious deeply-bound states at large  $\Lambda$ . In other channels we must deal with short-range hard-core repulsion becoming more prominent and producing fluctuating sign or complex phase cancellations. The general connection between sign/phase oscillations and repulsive interactions has been discussed in the literature in several different contexts [27, 28, 29]. The severity of the sign/phase problem scales exponentially with system size and strength of the repulsive interaction.

In order to avoid these difficulties we set the cutoff momentum  $\Lambda$  as low as possible for describing physical momenta up to  $m_\pi$ . We take  $\Lambda = 314 \text{ MeV} \approx 2.3m_\pi$ , corresponding with  $a^{-1} = 100 \text{ MeV}$ . This coarse lattice approach is similar in motivation to the continuum low-momentum potential  $V_{\text{low } k}$  derived using the renormalization group [30, 31]. There has been some discussion in the literature about the consistency of the Weinberg power counting scheme at high momentum cutoff, starting with the work of [32, 33] and more recently [34, 35, 36, 37, 38]. Due to the computational reasons explained above, we are prevented from reaching high momentum cutoff scales in our lattice calculations where alternative power counting schemes may be useful.

For nearly all  $|q| < \Lambda$  we can expand the two-pion exchange potential in powers of  $q^2/(4m_\pi^2)$ ,

$$L(q) = 1 + \frac{1}{3} \frac{q^2}{4m_\pi^2} + \dots, \quad (9)$$

$$\frac{4m_\pi^2}{4m_\pi^2 + q^2} L(q) = 1 - \frac{2}{3} \frac{q^2}{4m_\pi^2} + \dots, \quad (10)$$

$$V_{\text{NLO}}^{\text{TPEP}} = -\frac{\boldsymbol{\tau}_1 \cdot \boldsymbol{\tau}_2}{384\pi^2 f_\pi^4} \left[ 4m_\pi^2 (8g_A^4 - 4g_A^2 - 1) + \frac{2}{3} q^2 (34g_A^4 - 17g_A^2 - 2) + O\left(\left(\frac{q^2}{4m_\pi^2}\right)^2\right) \right] \\ - \frac{3g_A^4}{64\pi^2 f_\pi^4} [(\vec{q} \cdot \vec{\sigma}_1)(\vec{q} \cdot \vec{\sigma}_2) - q^2(\vec{\sigma}_1 \cdot \vec{\sigma}_2)] \left[ 1 + O\left(\frac{q^2}{4m_\pi^2}\right) \right]. \quad (11)$$

This expansion fails to converge only for values of  $q$  near the cutoff scale  $\Lambda \approx 2.3m_\pi$ , where the effective theory is already problematic due to large cutoff effects of size  $O(q^2/\Lambda^2)$ . From a practical viewpoint there is no need to keep the full non-local structure of  $V_{\text{NLO}}^{\text{TPEP}}$  at this lattice spacing. Instead we simply use

$$V_{\text{LO}} = V^{(0)} + V^{\text{OPEP}}, \quad (12)$$

$$V_{\text{NLO}} = V_{\text{LO}} + \Delta V^{(0)} + V^{(2)}, \quad (13)$$

where the terms in Eq. (11) with up to two powers of  $q$  are absorbed as a redefinition of the coefficients  $\Delta V^{(0)}$  and  $V^{(2)}$ . This same approach can be applied to the two-pion exchange potential at next-to-next-to-leading order (NNLO) and higher-order  $n$ -pion exchange potentials.

### C. Model independence at fixed lattice spacing

The usual test of model independence in low-energy effective field theory calculations is to check for sensitivity on the cutoff scale  $\Lambda$ . The difference between calculations at a given order for two different cutoff scales  $\Lambda_1$  and  $\Lambda_2$  should be no larger than the omitted corrections at the next order. On the lattice this test is problematic since we cannot change the lattice spacing by a large amount due to computational constraints. Fortunately cutoff independence is just one of many ways to test model independence. In the following we discuss a general class of methods to check model independence at fixed lattice spacing.

Let us use the notation  $V^{Q^n/\Lambda^n}$  to denote two-nucleon operators with the following properties.  $V^{Q^n/\Lambda^n}$  is a sum of local two-nucleon interactions each with at least  $n$  powers of momenta and an analytic function of momenta below the cutoff scale  $\Lambda$ . We use the adjective “quasi-local” to describe  $V^{Q^n/\Lambda^n}$  since the interactions are purely short range. Quasi-local operators of this type arise naturally in improved lattice actions of the type considered in [13].

At fixed lattice spacing we consider two modified lowest-order actions of the form

$$V_{\text{LO}_1} = V_1^{(0)} + V^{\text{OPEP}} + V_1^{Q^2/\Lambda^2}, \quad (14)$$

$$V_{\text{LO}_2} = V_2^{(0)} + V^{\text{OPEP}} + V_2^{Q^2/\Lambda^2}, \quad (15)$$

where  $V_1^{Q^2/\Lambda^2}$  and  $V_2^{Q^2/\Lambda^2}$  are different quasi-local operators with at least two powers of momenta. The leading-order interactions are iterated nonperturbatively and so, when fitted to physical low-energy data, the contact terms  $V_1^{(0)}$  and  $V_2^{(0)}$  in general have different coefficients. However we expect low-energy physical observables such as scattering phase shifts, binding energies, etc., should agree up to differences comparable to the omitted NLO corrections.

Similarly at NLO we may consider modified actions of the form

$$V_{\text{NLO}_1} = V_{\text{LO}_1} + \Delta V_1^{(0)} + V_1^{(2)} + V_1^{Q^4/\Lambda^4}, \quad (16)$$

$$V_{\text{NLO}_2} = V_{\text{LO}_2} + \Delta V_2^{(0)} + V_2^{(2)} + V_2^{Q^4/\Lambda^4}, \quad (17)$$

where  $V_1^{Q^4/\Lambda^4}$  and  $V_2^{Q^4/\Lambda^4}$  are different quasi-local operators with at least four powers of momenta. Once again low-energy physical observables should agree up to differences comparable to the omitted corrections at the next order.

At any given order the effect of small changes of the lattice spacing can be reinterpreted at fixed lattice spacing as a renormalization group transformation on higher-order local operator coefficients. In principle this type of modification is covered by our condition of model independence for general  $V^{Q^n/\Lambda^n}$ . Nevertheless it is good to check explicitly as many variations as possible, and studies at different lattice spacings as well as different functional forms for  $V^{Q^n/\Lambda^n}$  are planned for the future.

### III. LATTICE FORMALISM

#### A. Lattice notation and cubic symmetries

In this paper we assume exact isospin symmetry and neglect electromagnetic interactions. We use  $\vec{n}$  to represent integer-valued lattice vectors on a three-dimensional spatial lattice and either  $\vec{p}$ ,  $\vec{q}$ , or  $\vec{k}$  to represent integer-valued momentum lattice vectors.  $\hat{l} = \hat{1}, \hat{2}, \hat{3}$  are unit lattice vectors in the spatial directions,  $a$  is the spatial lattice spacing, and  $L$  is the length of the cubic spatial lattice in each direction. We use the Euclidean transfer matrix formalism defined in [13] with lattice time step  $a_t$ , and the integer  $n_t$  labels the time steps. We define  $\alpha_t$  as the ratio between lattice spacings,  $\alpha_t = a_t/a$ . Throughout we use dimensionless parameters and operators, which correspond with physical values multiplied by the appropriate power of  $a$ . Final results are presented in physical units with the corresponding unit stated explicitly. As in [13] we use the spatial lattice spacing  $a = (100 \text{ MeV})^{-1}$  and temporal lattice spacing  $a_t = (70 \text{ MeV})^{-1}$ .

We use  $a$  and  $a^\dagger$  to denote annihilation and creation operators. To avoid confusion we

TABLE I: Irreducible  $\text{SO}(3, \mathbb{Z})$  representations

Representation	$J_z$	Example
$A_1$	$0 \bmod 4$	$Y_{0,0}$
$T_1$	$0, 1, 3 \bmod 4$	$\{Y_{1,0}, Y_{1,1}, Y_{1,-1}\}$
$E$	$0, 2 \bmod 4$	$\left\{Y_{2,0}, \frac{Y_{2,-2} + Y_{2,2}}{\sqrt{2}}\right\}$
$T_2$	$1, 2, 3 \bmod 4$	$\left\{Y_{2,1}, \frac{Y_{2,-2} - Y_{2,2}}{\sqrt{2}}, Y_{2,-1}\right\}$
$A_2$	$2 \bmod 4$	$\frac{Y_{3,2} - Y_{3,-2}}{\sqrt{2}}$

make explicit in our lattice notation all spin and isospin indices using

$$a_{0,0} = a_{\uparrow,p}, \quad a_{0,1} = a_{\uparrow,n}, \quad (18)$$

$$a_{1,0} = a_{\downarrow,p}, \quad a_{1,1} = a_{\downarrow,n}. \quad (19)$$

The first subscript is for spin and the second subscript is for isospin. We use  $\tau_I$  with  $I = 1, 2, 3$  to represent Pauli matrices acting in isospin space and  $\sigma_S$  with  $S = 1, 2, 3$  to represent Pauli matrices acting in spin space. We also use the letters  $S$  and  $I$  to denote the total spin and total isospin for the two-nucleon system. The intended meaning in each case should be clear from the context.

On the lattice the rotational symmetry is reduced to the cubic subgroup  $\text{SO}(3, \mathbb{Z})$  of  $\text{SO}(3)$  while isospin symmetry remains intact as the full  $\text{SU}(2)$  symmetry. There are five irreducible representations of the cubic rotational group. These are usually written as  $A_1$ ,  $T_1$ ,  $E$ ,  $T_2$ , and  $A_2$ . Some of their properties and examples in terms of spherical harmonics  $Y_{L,L_z}(\theta, \phi)$  are listed in Table I. The  $2J + 1$  elements of the total angular momentum  $J$  representation of  $\text{SO}(3)$  break up into smaller pieces consisting of the five irreducible representations.

We use the eight vertices of a unit cube on the lattice to define spatial derivatives. For each spatial direction  $l = 1, 2, 3$  and any lattice function  $f(\vec{n})$ , let

$$\Delta_l f(\vec{n}) = \frac{1}{4} \sum_{\nu_1, \nu_2, \nu_3=0,1} (-1)^{\nu_1+1} f(\vec{n} + \vec{\nu}), \quad \vec{\nu} = \nu_1 \hat{1} + \nu_2 \hat{2} + \nu_3 \hat{3}. \quad (20)$$

We also define the double spatial derivative along direction  $l$ ,

$$\nabla_l^2 f(\vec{n}) = f(\vec{n} + \hat{l}) + f(\vec{n} - \hat{l}) - 2f(\vec{n}). \quad (21)$$

## B. Densities and current densities

We define the local density,

$$\rho^{a^\dagger, a}(\vec{n}) = \sum_{i,j=0,1} a_{i,j}^\dagger(\vec{n}) a_{i,j}(\vec{n}), \quad (22)$$

which is invariant under Wigner's SU(4) symmetry [39]. Similarly we define the local spin density for  $S = 1, 2, 3$ ,

$$\rho_S^{a^\dagger, a}(\vec{n}) = \sum_{i,j,i'=0,1} a_{i,j}^\dagger(\vec{n}) [\sigma_S]_{ii'} a_{i',j}(\vec{n}), \quad (23)$$

isospin density for  $I = 1, 2, 3$ ,

$$\rho_I^{a^\dagger, a}(\vec{n}) = \sum_{i,j,j'=0,1} a_{i,j}^\dagger(\vec{n}) [\tau_I]_{jj'} a_{i,j'}(\vec{n}), \quad (24)$$

and spin-isospin density for  $S, I = 1, 2, 3$ ,

$$\rho_{S,I}^{a^\dagger, a}(\vec{n}) = \sum_{i,j,i',j'=0,1} a_{i,j}^\dagger(\vec{n}) [\sigma_S]_{ii'} [\tau_I]_{jj'} a_{i',j'}(\vec{n}). \quad (25)$$

For each static density we also have an associated current density. Similar to the definition of the lattice derivative  $\Delta_l$  in Eq. (20), we use the eight vertices of a unit cube,

$$\vec{\nu} = \nu_1 \hat{1} + \nu_2 \hat{2} + \nu_3 \hat{3}, \quad (26)$$

for  $\nu_1, \nu_2, \nu_3 = 0, 1$ . Let  $\vec{\nu}(-l)$  for  $l = 1, 2, 3$  be the result of reflecting the  $l^{\text{th}}$ -component of  $\vec{\nu}$  about the center of the cube,

$$\vec{\nu}(-l) = \vec{\nu} + (1 - 2\nu_l) \hat{l}. \quad (27)$$

Omitting factors of  $i$  and  $1/m$ , we can write the  $l^{\text{th}}$ -component of the SU(4)-invariant current density as

$$\Pi_l^{a^\dagger, a}(\vec{n}) = \frac{1}{4} \sum_{\nu_1, \nu_2, \nu_3=0,1} \sum_{i,j=0,1} (-1)^{\nu_l+1} a_{i,j}^\dagger(\vec{n} + \vec{\nu}(-l)) a_{i,j}(\vec{n} + \vec{\nu}). \quad (28)$$

Similarly the  $l^{\text{th}}$ -component of spin current density is

$$\Pi_{l,S}^{a^\dagger, a}(\vec{n}) = \frac{1}{4} \sum_{\nu_1, \nu_2, \nu_3=0,1} \sum_{i,j,i'=0,1} (-1)^{\nu_l+1} a_{i,j}^\dagger(\vec{n} + \vec{\nu}(-l)) [\sigma_S]_{ii'} a_{i',j}(\vec{n} + \vec{\nu}), \quad (29)$$

$l^{\text{th}}$ -component of isospin current density is

$$\Pi_{l,I}^{a^\dagger, a}(\vec{n}) = \frac{1}{4} \sum_{\nu_1, \nu_2, \nu_3=0,1} \sum_{i,j,j'=0,1} (-1)^{\nu_l+1} a_{i,j}^\dagger(\vec{n} + \vec{\nu}(-l)) [\tau_I]_{jj'} a_{i,j'}(\vec{n} + \vec{\nu}), \quad (30)$$



and  $l^{\text{th}}$ -component of spin-isospin current density is

$$\Pi_{l,S,I}^{a^\dagger,a}(\vec{n}) = \frac{1}{4} \sum_{\nu_1,\nu_2,\nu_3=0,1} \sum_{i,j,i',j'=0,1} (-1)^{\nu_1+1} a_{i,j}^\dagger(\vec{n} + \vec{\nu}(-l)) [\sigma_S]_{ii'} [\tau_I]_{jj'} a_{i',j'}(\vec{n} + \vec{\nu}). \quad (31)$$

### C. Instantaneous free pion action

The lattice action for free pions with purely instantaneous propagation is

$$S_{\pi\pi}(\pi_I) = \alpha_t \left( \frac{m_\pi^2}{2} + 3 \right) \sum_{\vec{n}, n_t, I} \pi_I(\vec{n}, n_t) \pi_I(\vec{n}, n_t) - \alpha_t \sum_{\vec{n}, n_t, I, l} \pi_I(\vec{n}, n_t) \pi_I(\vec{n} + \hat{l}, n_t), \quad (32)$$

where  $\pi_I$  is the pion field labelled with isospin index  $I$ . We note that pion fields at different time steps  $n_t$  and  $n'_t$  are decoupled due to the omission of time derivatives. This generates instantaneous propagation at each time step when computing one-pion exchange diagrams. It is convenient to define a rescaled pion field,  $\pi'_I$ ,

$$\pi'_I(\vec{n}, n_t) = \sqrt{q_\pi} \pi_I(\vec{n}, n_t), \quad (33)$$

$$q_\pi = \alpha_t (m_\pi^2 + 6). \quad (34)$$

Then

$$S_{\pi\pi}(\pi'_I) = \frac{1}{2} \sum_{\vec{n}, n_t, I} \pi'_I(\vec{n}, n_t) \pi'_I(\vec{n}, n_t) - \frac{\alpha_t}{q_\pi} \sum_{\vec{n}, n_t, I, l} \pi'_I(\vec{n}, n_t) \pi'_I(\vec{n} + \hat{l}, n_t). \quad (35)$$

In momentum space the action is

$$S_{\pi\pi}(\pi'_I) = \frac{1}{L^3} \sum_{I, \vec{k}} \pi'_I(-\vec{k}, n_t) \pi'_I(\vec{k}, n_t) \left[ \frac{1}{2} - \frac{\alpha_t}{q_\pi} \sum_l \cos\left(\frac{2\pi k_l}{L}\right) \right]. \quad (36)$$

The instantaneous pion correlation function at spatial separation  $\vec{n}$  is

$$\begin{aligned} \left\langle \pi'_I(\vec{n}, n_t) \pi'_I(\vec{0}, n_t) \right\rangle &= \frac{\int D\pi'_I \pi'_I(\vec{n}, n_t) \pi'_I(\vec{0}, n_t) \exp[-S_{\pi\pi}]}{\int D\pi'_I \exp[-S_{\pi\pi}]} \quad (\text{no sum on } I) \\ &= \frac{1}{L^3} \sum_{\vec{k}} e^{-i\frac{2\pi}{L}\vec{k}\cdot\vec{n}} D_\pi(\vec{k}), \end{aligned} \quad (37)$$

where

$$D_\pi(\vec{k}) = \frac{1}{1 - \frac{2\alpha_t}{q_\pi} \sum_l \cos\left(\frac{2\pi k_l}{L}\right)}. \quad (38)$$

It is useful also to define the two-derivative pion correlator,  $G_{S_1 S_2}(\vec{n})$ ,

$$\begin{aligned} G_{S_1 S_2}(\vec{n}) &= \left\langle \Delta_{S_1} \pi'_I(\vec{n}, n_t) \Delta_{S_2} \pi'_I(\vec{0}, n_t) \right\rangle \quad (\text{no sum on } I) \\ &= \frac{1}{16} \sum_{\nu_1,\nu_2,\nu_3=0,1} \sum_{\nu'_1,\nu'_2,\nu'_3=0,1} (-1)^{\nu_{S_1}} (-1)^{\nu'_{S_2}} \left\langle \pi'_I(\vec{n} + \vec{\nu} - \vec{\nu}', n_t) \pi'_I(\vec{0}, n_t) \right\rangle. \end{aligned} \quad (39)$$

## IV. LATTICE TRANSFER MATRICES

### A. Leading-order actions LO<sub>1</sub> and LO<sub>2</sub>

The analysis in [13] considers the lattice path integral with and without auxiliary fields as well as the lattice transfer matrix with and without auxiliary fields. All four formulations are shown to be exactly the same. Here we discuss only the lattice transfer matrix without auxiliary fields. This formulation is the most useful for calculating nucleon-nucleon scattering phase shifts and mixing angles. In simple terms the Euclidean transfer matrix is the exponential of the Hamiltonian  $\exp(-H\Delta t)$ , where  $\Delta t$  equals one temporal lattice spacing. For example we can write the free-nucleon transfer matrix as

$$M_{\text{free}} \equiv: \exp(-H_{\text{free}}\alpha_t) : , \quad (40)$$

where the  $::$  symbols indicate normal ordering. We use the  $O(a^4)$ -improved free lattice Hamiltonian,

$$\begin{aligned} H_{\text{free}} = & \frac{49}{12m} \sum_{\vec{n}} \sum_{i,j=0,1} a_{i,j}^\dagger(\vec{n}) a_{i,j}(\vec{n}) \\ & - \frac{3}{4m} \sum_{\vec{n}} \sum_{i,j=0,1} \sum_{l=1,2,3} \left[ a_{i,j}^\dagger(\vec{n}) a_{i,j}(\vec{n} + \hat{l}) + a_{i,j}^\dagger(\vec{n}) a_{i,j}(\vec{n} - \hat{l}) \right] \\ & + \frac{3}{40m} \sum_{\vec{n}} \sum_{i,j=0,1} \sum_{l=1,2,3} \left[ a_{i,j}^\dagger(\vec{n}) a_{i,j}(\vec{n} + 2\hat{l}) + a_{i,j}^\dagger(\vec{n}) a_{i,j}(\vec{n} - 2\hat{l}) \right] \\ & - \frac{1}{180m} \sum_{\vec{n}} \sum_{i,j=0,1} \sum_{l=1,2,3} \left[ a_{i,j}^\dagger(\vec{n}) a_{i,j}(\vec{n} + 3\hat{l}) + a_{i,j}^\dagger(\vec{n}) a_{i,j}(\vec{n} - 3\hat{l}) \right]. \end{aligned} \quad (41)$$

With the interactions included we take the standard lattice transfer matrix defined in [13] for LO<sub>1</sub>,

$$\begin{aligned} M_{\text{LO}_1} \equiv: & \exp \left\{ -H_{\text{free}}\alpha_t - \frac{1}{2}C\alpha_t \sum_{\vec{n}} \left[ \rho^{a^\dagger, a}(\vec{n}) \right]^2 - \frac{1}{2}C_{I^2}\alpha_t \sum_I \sum_{\vec{n}} \left[ \rho_I^{a^\dagger, a}(\vec{n}) \right]^2 \right. \\ & \left. + \frac{g_A^2 \alpha_t^2}{8f_\pi^2 q_\pi} \sum_{S_1, S_2, I} \sum_{\vec{n}_1, \vec{n}_2} G_{S_1 S_2}(\vec{n}_1 - \vec{n}_2) \rho_{S_1, I}^{a^\dagger, a}(\vec{n}_1) \rho_{S_2, I}^{a^\dagger, a}(\vec{n}_2) \right\} : . \end{aligned} \quad (42)$$

where  $C$  is the coefficient of the Wigner SU(4)-invariant contact interaction and  $C_{I^2}$  is the coefficient of the isospin-dependent contact interaction. For  $C$  and  $C_{I^2}$  we use the values

$$C = (3C^{I=1} + C^{I=0}) / 4, \quad (43)$$

$$C_{I^2} = (C^{I=1} - C^{I=0}) / 4, \quad (44)$$

with  $C^{I=1} = -5.021 \times 10^{-5} \text{ MeV}^{-2}$  and  $C^{I=0} = -5.714 \times 10^{-5} \text{ MeV}^{-2}$ .

For the  $\text{LO}_2$  transfer matrix we use the improved lattice transfer matrix defined in [13],

$$M_{\text{LO}_2} \equiv: \exp \left\{ -H_{\text{free}} \alpha_t - \frac{\alpha_t}{2L^3} \sum_{\vec{q}} f(q^2) \left[ C \rho^{a^\dagger, a}(\vec{q}) \rho^{a^\dagger, a}(-\vec{q}) + C_{I^2} \sum_I \rho_I^{a^\dagger, a}(\vec{q}) \rho_I^{a^\dagger, a}(-\vec{q}) \right] \right. \\ \left. + \frac{g_A^2 \alpha_t^2}{8f_\pi^2 q_\pi} \sum_{S_1, S_2, I} \sum_{\vec{n}_1, \vec{n}_2} G_{S_1 S_2}(\vec{n}_1 - \vec{n}_2) \rho_{S_1, I}^{a^\dagger, a}(\vec{n}_1) \rho_{S_2, I}^{a^\dagger, a}(\vec{n}_2) \right\} :. \quad (45)$$

where the momentum-dependent coefficient function  $f(q^2)$  is defined as

$$f(q^2) = f_0^{-1} \exp \left[ -b \sum_l (1 - \cos q_l) \right], \quad (46)$$

and the normalization factor  $f_0$  is determined by the condition

$$f_0 = \frac{1}{L^3} \sum_{\vec{q}} \exp \left[ -b \sum_l (1 - \cos q_l) \right]. \quad (47)$$

As in [13] we use the value  $b = 0.6$ . This gives approximately the correct average effective range for the two  $S$ -wave channels when  $C$  and  $C_{I^2}$  are properly tuned. For  $C$  and  $C_{I^2}$  we use  $C^{I=1} = -3.414 \times 10^{-5} \text{ MeV}^{-2}$  and  $C^{I=0} = -4.780 \times 10^{-5} \text{ MeV}^{-2}$  and the relations in Eq. (43) and (44). More details on these leading-order actions can be found in [13].

## B. Next-to-leading-order actions $\text{NLO}_1$ and $\text{NLO}_2$

For the next-to-leading-order transfer matrices  $M_{\text{NLO}_1}$  and  $M_{\text{NLO}_2}$  we add the following local interactions to the leading-order transfer matrices  $M_{\text{LO}_1}$  and  $M_{\text{LO}_2}$ . We first start with corrections to the leading-order contact interactions. These can be written as

$$\Delta V = \frac{1}{2} \Delta C : \sum_{\vec{n}} \rho^{a^\dagger, a}(\vec{n}) \rho^{a^\dagger, a}(\vec{n}) :, \quad (48)$$

$$\Delta V_{I^2} = \frac{1}{2} \Delta C_{I^2} : \sum_{\vec{n}, I} \rho_I^{a^\dagger, a}(\vec{n}) \rho_I^{a^\dagger, a}(\vec{n}) :. \quad (49)$$

At next-to-leading order there are seven independent contact interactions with two derivatives. These can be written as

$$V_{q^2} = -\frac{1}{2} C_{q^2} : \sum_{\vec{n}, l} \rho^{a^\dagger, a}(\vec{n}) \nabla_l^2 \rho^{a^\dagger, a}(\vec{n}) :, \quad (50)$$

$$V_{I^2,q^2} = -\frac{1}{2}C_{I^2,q^2} : \sum_{\vec{n},I,l} \rho_I^{a^\dagger,a}(\vec{n}) \nabla_l^2 \rho_I^{a^\dagger,a}(\vec{n}) :, \quad (51)$$

$$V_{S^2,q^2} = -\frac{1}{2}C_{S^2,q^2} : \sum_{\vec{n},S,l} \rho_S^{a^\dagger,a}(\vec{n}) \nabla_l^2 \rho_S^{a^\dagger,a}(\vec{n}) :, \quad (52)$$

$$V_{S^2,I^2,q^2} = -\frac{1}{2}C_{S^2,I^2,q^2} : \sum_{\vec{n},S,I,l} \rho_{S,I}^{a^\dagger,a}(\vec{n}) \nabla_l^2 \rho_{S,I}^{a^\dagger,a}(\vec{n}) :, \quad (53)$$

$$V_{(q \cdot S)^2} = \frac{1}{2}C_{(q \cdot S)^2} : \sum_{\vec{n}} \sum_S \Delta_S \rho_S^{a^\dagger,a}(\vec{n}) \sum_{S'} \Delta_{S'} \rho_{S'}^{a^\dagger,a}(\vec{n}) :, \quad (54)$$

$$V_{I^2,(q \cdot S)^2} = \frac{1}{2}C_{I^2,(q \cdot S)^2} : \sum_{\vec{n},I} \sum_S \Delta_S \rho_{S,I}^{a^\dagger,a}(\vec{n}) \sum_{S'} \Delta_{S'} \rho_{S',I}^{a^\dagger,a}(\vec{n}) :, \quad (55)$$

$$V_{(iq \times S) \cdot k} = -\frac{i}{2}C_{(iq \times S) \cdot k} : \sum_{\vec{n},l,S,l'} \varepsilon_{l,S,l'} \left[ \Pi_l^{a^\dagger,a}(\vec{n}) \Delta_{l'} \rho_S^{a^\dagger,a}(\vec{n}) + \Pi_{l,S}^{a^\dagger,a}(\vec{n}) \Delta_{l'} \rho^{a^\dagger,a}(\vec{n}) \right] : . \quad (56)$$

The subscripts indicate the continuum limit of the interactions. A detailed discussion of the continuum limit for each of these NLO lattice interactions is given in the appendix.

The  $V_{(iq \times S) \cdot k}$  term corresponds with the continuum interaction

$$C_{(iq \times S) \cdot k} (i\vec{q} \times (\vec{\sigma}_1 + \vec{\sigma}_2)) \cdot \vec{k}. \quad (57)$$

We note that this interaction vanishes unless the total spin  $S = 1$ . We note also that the continuum limit of the interaction is antisymmetric under the exchange of  $\vec{q}$  and  $\vec{k}$ . Therefore the continuum interaction is nonzero only for odd parity channels. Unfortunately the lattice interaction  $V_{(iq \times S) \cdot k}$  does not share this exact  $t$ - $u$  channel antisymmetry at nonzero lattice spacing. Therefore  $V_{(iq \times S) \cdot k}$  produces small lattice artifacts for  $S = 1$  in even parity channels. Fortunately in this case there is a simple way to remove them. We include an explicit projection onto total isospin  $I = 1$ ,

$$V_{(iq \times S) \cdot k}^{I=1} = -\frac{i}{2}C_{(iq \times S) \cdot k}^{I=1} \left\{ \frac{3}{4} : \sum_{\vec{n},l,S,l'} \varepsilon_{l,S,l'} \left[ \Pi_l^{a^\dagger,a}(\vec{n}) \Delta_{l'} \rho_S^{a^\dagger,a}(\vec{n}) + \Pi_{l,S}^{a^\dagger,a}(\vec{n}) \Delta_{l'} \rho^{a^\dagger,a}(\vec{n}) \right] : \right. \\ \left. + \frac{1}{4} : \sum_{\vec{n},l,S,l',I} \varepsilon_{l,S,l',I} \left[ \Pi_{l,I}^{a^\dagger,a}(\vec{n}) \Delta_{l'} \rho_{S,I}^{a^\dagger,a}(\vec{n}) + \Pi_{l,S,I}^{a^\dagger,a}(\vec{n}) \Delta_{l'} \rho_I^{a^\dagger,a}(\vec{n}) \right] : \right\}. \quad (58)$$

In the continuum limit the interaction is already pure  $I = 1$  due to total antisymmetry, and so the isospin triplet projection has no effect. At nonzero lattice spacing this projection completely eliminates lattice artifacts in the  $S = 1$  even parity channels.

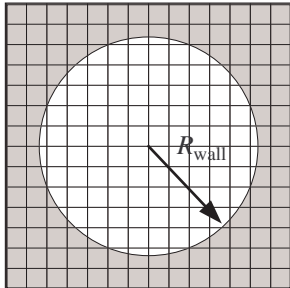


FIG. 1: Spherical wall imposed in the center-of-mass frame.

## V. TWO-NUCLEON SCATTERING ON THE LATTICE

### A. Spherical wall method

We measure phase shifts by imposing a hard spherical wall boundary on the relative separation between the two nucleons at some chosen radius  $R_{\text{wall}}$  [17]. The spherical wall removes copies of the interactions due to the periodic boundaries of the lattice. Viewed in the center-of-mass frame we solve the Schrödinger equation for spherical standing waves which vanish at  $r = R_{\text{wall}}$  as indicated in Fig. 1.

In the spin singlet case for values of  $r$  beyond the range of the interaction, the spherical standing wave can be decomposed as a superposition of products of spherical harmonics and spherical Bessel functions. Explicitly we have

$$[\cos \delta_L \cdot j_L(kr) - \sin \delta_L \cdot y_L(kr)] Y_{L,L_z}(\theta, \phi), \quad (59)$$

where the center-of-mass energy of the spherical wave is

$$E = 2 \frac{k^2}{2m} = \frac{k^2}{m}, \quad (60)$$

and the phase shift for partial wave  $L$  is  $\delta_L$ . Therefore we know  $k$  from the energy  $E$ , and the phase shift  $\delta_L$  is determined by setting the wavefunction in Eq. (59) equal to zero at the wall boundary,

$$\cos \delta_L \cdot j_L(kR_{\text{wall}}) = \sin \delta_L \cdot y_L(kR_{\text{wall}}), \quad (61)$$

$$\delta_L = \tan^{-1} \left[ \frac{j_L(kR_{\text{wall}})}{y_L(kR_{\text{wall}})} \right]. \quad (62)$$

On the lattice there is some ambiguity on the precise value of  $R_{\text{wall}}$  since the components of  $\vec{r}$  must be integer multiples of the lattice spacing. We resolve this ambiguity by fine-tuning the value of  $R_{\text{wall}}$  for each standing wave so that  $\delta_L$  equals zero when the particles are non-interacting.

For the spin triplet case, however, spin-orbit coupling produces mixing between partial waves  $L = J - 1$  and  $L = J + 1$ . If we use the two-component notation,

$$\begin{bmatrix} R_{J-1}(r) \\ R_{J+1}(r) \end{bmatrix}, \quad (63)$$

for the radial part of the wavefunction, then we find two sets of standing wave solutions of the form

$$\Psi^I \propto \frac{1}{k^I r} \begin{bmatrix} A_{J-1}^I \sin(k^I r - \frac{J-1}{2}\pi + \Delta_{J-1}^I) \\ A_{J+1}^I \sin(k^I r - \frac{J+1}{2}\pi + \Delta_{J+1}^I) \end{bmatrix} \quad (64)$$

at energy  $E^I = (k^I)^2/m$  and

$$\Psi^{II} \propto \frac{1}{k^{II} r} \begin{bmatrix} A_{J-1}^{II} \sin(k^{II} r - \frac{J-1}{2}\pi + \Delta_{J-1}^{II}) \\ A_{J+1}^{II} \sin(k^{II} r - \frac{J+1}{2}\pi + \Delta_{J+1}^{II}) \end{bmatrix} \quad (65)$$

at  $E^{II} = (k^{II})^2/m$ . These can be used to derive the phase shifts  $\delta_{J-1}$  and  $\delta_{J+1}$  and mixing angle  $\varepsilon_J$  [17],

$$\tan(-\Delta_{J-1}^I + \delta_{J-1}) \tan(-\Delta_{J+1}^I + \delta_{J+1}) = \tan^2 \varepsilon_J, \quad (66)$$

$$\tan(-\Delta_{J-1}^{II} + \delta_{J-1}) \tan(-\Delta_{J+1}^{II} + \delta_{J+1}) = \tan^2 \varepsilon_J, \quad (67)$$

$$A_{J-1}^I \tan \varepsilon_J = -A_{J+1}^I \frac{\sin(-\Delta_{J+1}^I + \delta_{J+1})}{\cos(-\Delta_{J-1}^I + \delta_{J-1})}, \quad (68)$$

$$A_{J-1}^{II} \tan \varepsilon_J = -A_{J+1}^{II} \frac{\sin(-\Delta_{J+1}^{II} + \delta_{J+1})}{\cos(-\Delta_{J-1}^{II} + \delta_{J-1})}. \quad (69)$$

The phase shifts and mixing angle in Eq. (66) and (68) are at momentum  $k^I$  while the phase shifts and mixing angle in Eq. (67) and (69) are at momentum  $k^{II}$ . We therefore consider only close pairs of values  $k^I \approx k^{II}$  in solving Eq. (66)-(69). This can be done for example by considering the  $(n+1)^{\text{st}}$ -radial excitation of  $L = J - 1$  together with the  $n^{\text{th}}$ -radial excitation of  $L = J + 1$ . In this scheme we use

$$\tan(-\Delta_{J-1}^I + \delta_{J-1}(k^I)) \tan(-\Delta_{J+1}^I + \delta_{J+1}(k^I)) = \tan^2 [\varepsilon_J(k^I)], \quad (70)$$

$$\tan(-\Delta_{J-1}^{II} + \delta_{J-1}(k^I)) \tan(-\Delta_{J+1}^{II} + \delta_{J+1}(k^I)) \approx \tan^2 [\varepsilon_J(k^I)], \quad (71)$$

$$A_{J-1}^I \tan [\varepsilon_J(k^I)] = -A_{J+1}^I \frac{\sin(-\Delta_{J+1}^I + \delta_{J+1}(k^I))}{\cos(-\Delta_{J-1}^I + \delta_{J-1}(k^I))}, \quad (72)$$

for the phase shifts and mixing angle at  $k = k^I$ , and

$$\tan(-\Delta_{J-1}^I + \delta_{J-1}(k^{II})) \tan(-\Delta_{J+1}^I + \delta_{J+1}(k^{II})) \approx \tan^2 [\varepsilon_J(k^{II})], \quad (73)$$

$$\tan(-\Delta_{J-1}^{II} + \delta_{J-1}(k^{II})) \tan(-\Delta_{J+1}^{II} + \delta_{J+1}(k^{II})) = \tan^2 [\varepsilon_J(k^{II})], \quad (74)$$

$$A_{J-1}^{II} \tan [\varepsilon_J(k^{II})] = -A_{J+1}^{II} \frac{\sin(-\Delta_{J+1}^{II} + \delta_{J+1}(k^{II}))}{\cos(-\Delta_{J-1}^{II} + \delta_{J-1}(k^{II}))}, \quad (75)$$

for the phase shifts and mixing angle at  $k = k^{II}$ .

For momentum less than or equal to the pion mass all of the mixing angles  $\varepsilon_J$  are numerically small. It is therefore convenient to expand in powers of the mixing angle,

$$\delta_{J-1}(k^I) = \Delta_{J-1}^I + \frac{\varepsilon_J^2(k^I)}{\tan(-\Delta_{J+1}^I + \delta_{J+1}(k^I))} + O(\varepsilon_J^4), \quad (76)$$

$$\varepsilon_J(k^I) = -\frac{A_{J+1}^I}{A_{J-1}^I} \sin(\Delta_{J+1}^{II} - \Delta_{J+1}^I) + O(\varepsilon_J^3), \quad (77)$$

at  $k = k^I$  and

$$\delta_{J+1}(k^{II}) = \Delta_{J+1}^{II} + \frac{\varepsilon_J^2(k^{II})}{\tan(-\Delta_{J-1}^{II} + \delta_{J-1}(k^{II}))} + O(\varepsilon_J^4), \quad (78)$$

$$\varepsilon_J(k^{II}) = \frac{A_{J-1}^{II}}{A_{J+1}^{II}} \sin(\Delta_{J-1}^{II} - \Delta_{J-1}^I) + O(\varepsilon_J^3), \quad (79)$$

at  $k = k^{II}$ .

## B. LO energy levels and NLO corrections

In Fig. 2 we show energy levels for spin  $S = 0$  and isospin  $I = 1$  using lattice actions LO<sub>1</sub> and LO<sub>2</sub>. The spherical wall is at radius  $R_{\text{wall}} = 10 + \epsilon$  lattice units where  $\epsilon$  is a small positive number. We use this  $\epsilon$  notation to make explicit that  $|\vec{r}| = 10$  lattice units is inside the spherical wall but all lattice sites with  $|\vec{r}| > 10$  lattice units lie outside. The solid lines indicate the exact energy levels which reproduce data from the partial wave analysis of [40]. The energy levels for the standard action LO<sub>1</sub> are about 10% to 15% too low for the  $^1S_0$  states, while the improved action LO<sub>2</sub> is correct to within a couple of percent for all  $^1S_0$  states. Deviations for the higher partial waves are smaller than 1% for both LO<sub>1</sub> and LO<sub>2</sub>.

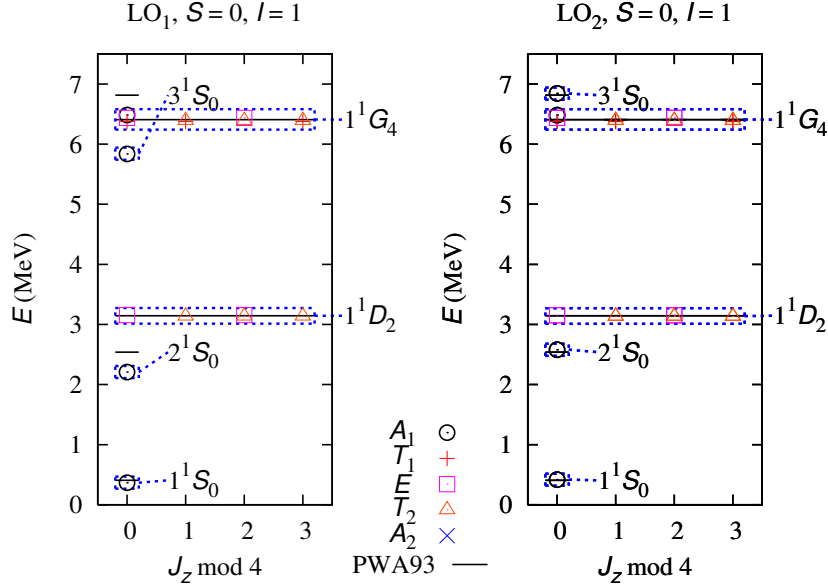


FIG. 2: Energy levels for  $S = 0$ ,  $I = 1$  using lattice actions  $LO_1$  and  $LO_2$  and a spherical wall at radius  $R_{\text{wall}} = 10 + \epsilon$  lattice units. The solid line indicates the exact energy levels which reproduce data from the partial wave analysis of [40].

The energy levels for spin  $S = 0$ , isospin  $I = 0$ , and  $R_{\text{wall}} = 10 + \epsilon$  lattice units are shown in Fig. 3. In this case  $LO_1$  is better for the  $^1P_1$  states and is within 1% of the exact values. The  $LO_2$  energy levels are further away, though still within 5% for the  $^1P_1$  states. The error for the  $^1F_3$  partial wave is much smaller than 1% for both  $LO_1$  and  $LO_2$ . Results for the  $LO_1$  and  $LO_2$  in the spin-triplet channels are similar in terms of their relative errors.

At next-to-leading order we have nine unknown operator coefficients to fit:  $\Delta C$ ,  $\Delta C_{I^2}$ ,  $C_{q^2}$ ,  $C_{I^2, q^2}$ ,  $C_{S^2, q^2}$ ,  $C_{S^2, I^2, q^2}$ ,  $C_{(q \cdot S)^2}$ ,  $C_{I^2, (q \cdot S)^2}$ , and  $C_{(iq \times S) \cdot k}^{I=1}$ . We fit these nine operator coefficients using the eight energy levels listed in Table II for  $R_{\text{wall}} = 10 + \epsilon$  lattice units, as well as the quadrupole moment of the deuteron  $Q_d$ . The deuteron quadrupole moment is a measure of the low-energy strength of  $S$ - $D$  partial wave mixing. We could instead use the mixing angle  $\varepsilon_1$  at some low momentum scale, but the quadrupole moment is actually an easier observable to compute. In this study we incorporate the nine NLO interactions using perturbation theory.



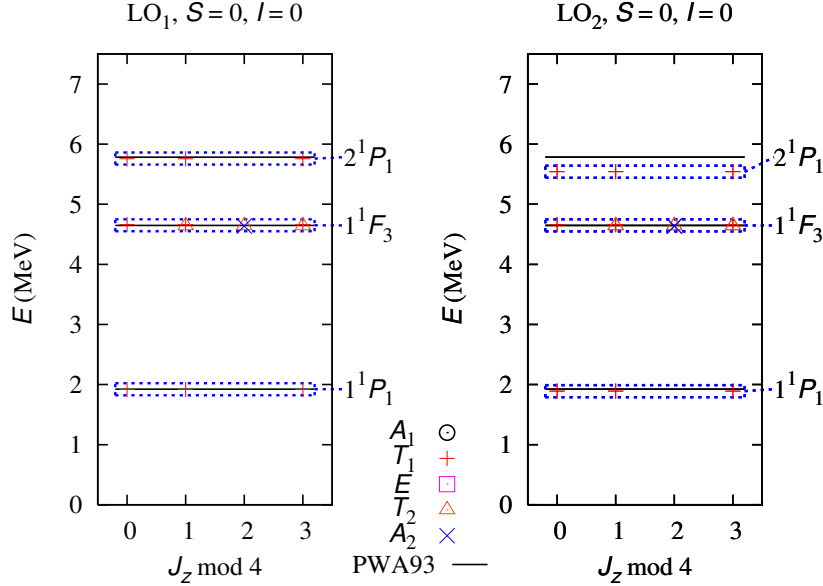


FIG. 3: Energy levels for  $S = 0$ ,  $I = 0$  using lattice actions  $\text{LO}_1$  and  $\text{LO}_2$  and a spherical wall at radius  $R_{\text{wall}} = 10 + \epsilon$  lattice units. The solid line indicates the exact energy levels which reproduce data from the partial wave analysis of [40].

The motivation for using perturbation theory for the NLO interactions is that it is computationally less expensive. Whether or not the NLO corrections can be treated using perturbation theory depends on the observable of interest. For example the standard action  $\text{LO}_1$  has a clustering instability which results in a strong overbinding of the alpha particle [13]. This instability is severe and probably cannot be fixed by introducing NLO corrections perturbatively. The problem is that the  $S$ -wave interactions are too attractive at momenta  $q \sim m_\pi$ , and the  $S$ -wave effective range corrections provided at NLO must be included nonperturbatively.

On the other hand the improved action  $\text{LO}_2$  resolves this problem using Gaussian smearing. The Gaussian-smearred interaction is contained in the term  $V_2^{Q^2/\Lambda^2}$  defined in Eq. (15). Since  $V_2^{Q^2/\Lambda^2}$  is iterated nonperturbatively along with rest of the leading-order action, the clustering instability is removed. We use this approach as a general strategy. The first attempt is to try a completely perturbative approach for all NLO corrections. If this fails

TABLE II: Results for LO<sub>1</sub> and LO<sub>2</sub> and target values

Spherical wave	Free nucleons	LO <sub>1</sub>	LO <sub>2</sub>	PWA93
$1^1S_0$ (MeV)	0.928	0.368	0.418	0.407
$3^1S_0$ (MeV)	8.535	5.838	6.843	6.815
$1^3S(D)_1$ (MeV)	0.928	-2.225	-2.225	-2.225
$3^3S(D)_1$ (MeV)	8.535	4.878	5.430	5.675
$2^1P_1$ (MeV)	5.691	5.755	5.541	5.782
$2^3P(F)_0$ (MeV)	5.691	5.569	5.396	5.584
$2^3P(F)_1$ (MeV)	5.691	5.754	5.652	5.753
$2^3P(F)_2$ (MeV)	5.691	5.684	5.558	5.669
$Q_d$ (fm <sup>2</sup> )	N/A	0.143	0.276	0.286

and some of the interactions must be handled nonperturbatively, then we include those interactions in the  $V^{Q^2/\Lambda^2}$  term in the leading-order action.

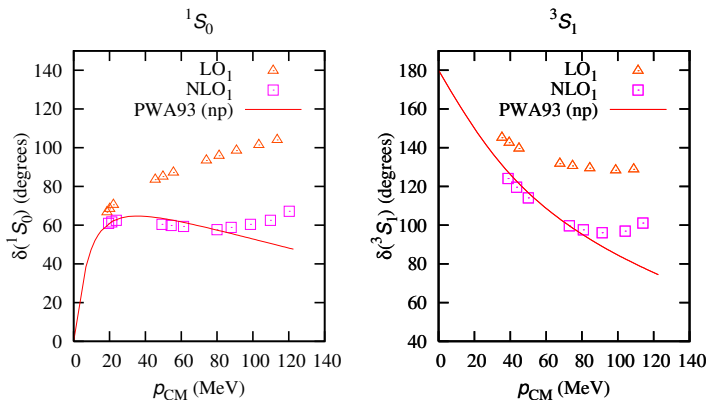
For each of the nine observables in Table II we compute the derivative with respect to each of the nine NLO coefficient operators. By inverting this  $9 \times 9$  Jacobian matrix we find the required values for the operator coefficients needed to match each of the observables using first-order perturbation theory. The results for the operator coefficients are shown in Table III. Although most of coefficients have generally the same order of magnitude and sign for NLO<sub>1</sub> and NLO<sub>2</sub>, we see that the coefficients in some cases are quite different.

## VI. RESULTS

We compute lattice phase shifts and mixing angles using spherical walls with radii  $R_{\text{wall}} = 10 + \epsilon$ ,  $9 + \epsilon$ , and  $8 + \epsilon$  lattice units. In order of increasing momentum, the lattice data corresponds with the first radial excitation for  $R_{\text{wall}} = 10 + \epsilon$ ,  $9 + \epsilon$ , and  $8 + \epsilon$ ; second radial excitation of  $R_{\text{wall}} = 10 + \epsilon$ ,  $9 + \epsilon$ , and  $8 + \epsilon$ ; and so on. The  $S$ -wave phase shifts for LO<sub>1</sub> and NLO<sub>1</sub> versus center-of-mass momentum  $p_{\text{CM}}$  are shown in Fig. 4. We compare these with the  $S$ -wave phase shifts for LO<sub>2</sub> and NLO<sub>2</sub> in Fig. 5. The NLO<sub>1</sub> and NLO<sub>2</sub> results are both in good agreement with partial wave results from [40]. Systematic errors are first noticeable at momenta greater than about 80 MeV and are larger for NLO<sub>1</sub>. In both

TABLE III: Results for NLO operator coefficients

Coefficient	NLO <sub>1</sub>	NLO <sub>2</sub>
$\Delta C$ (MeV <sup>-2</sup> )	$-1.43 \times 10^{-4}$	$-1.10 \times 10^{-5}$
$\Delta C_{I^2}$ (MeV <sup>-2</sup> )	$3.42 \times 10^{-5}$	$1.03 \times 10^{-5}$
$C_{q^2}$ (MeV <sup>-4</sup> )	$1.27 \times 10^{-9}$	$-1.01 \times 10^{-9}$
$C_{I^2, q^2}$ (MeV <sup>-4</sup> )	$-5.83 \times 10^{-10}$	$-4.07 \times 10^{-10}$
$C_{S^2, q^2}$ (MeV <sup>-4</sup> )	$-4.18 \times 10^{-12}$	$-1.72 \times 10^{-10}$
$C_{S^2, I^2, q^2}$ (MeV <sup>-4</sup> )	$-4.31 \times 10^{-10}$	$-2.81 \times 10^{-10}$
$C_{(q,S)^2}$ (MeV <sup>-4</sup> )	$-2.52 \times 10^{-11}$	$-3.23 \times 10^{-10}$
$C_{I^2, (q,S)^2}$ (MeV <sup>-4</sup> )	$6.24 \times 10^{-11}$	$1.43 \times 10^{-10}$
$C_{(iq \times S) \cdot k}^{I=1}$ (MeV <sup>-4</sup> )	$1.60 \times 10^{-10}$	$9.81 \times 10^{-11}$


 FIG. 4:  $S$ -wave phase shifts versus center-of-mass momentum for LO<sub>1</sub> and NLO<sub>1</sub>.

cases the deviations are consistent with higher-order effects such as two-nucleon contact interactions with four derivatives.

The  $P$ -wave phase shifts are presented in Fig. 6 and 7. The phase shifts are already not bad for LO<sub>1</sub> and are quite accurate for NLO<sub>1</sub>. This indicates that at low momenta only a small correction is needed on top of  $P$ -wave interactions produced by one-pion exchange. In the case of LO<sub>2</sub> we see that the effect of Gaussian smearing, while useful for  $S$ -wave phase shifts, produces an unphysical attraction in each  $P$ -wave channel that must be cancelled by

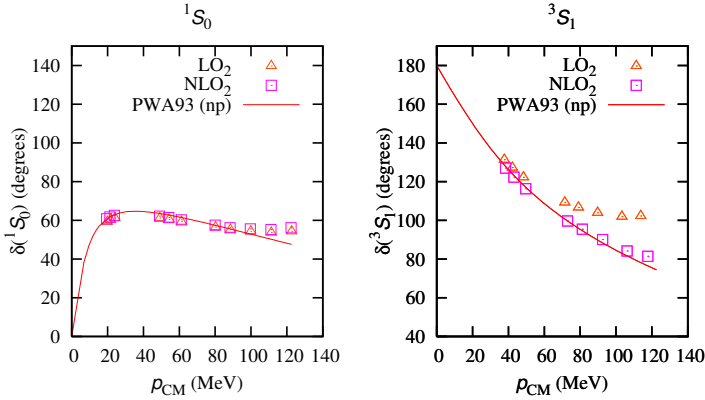


FIG. 5:  $S$ -wave phase shifts versus center-of-mass momentum for  $\text{LO}_2$  and  $\text{NLO}_2$ .

the  $\text{NLO}_2$  corrections. For the  $\text{NLO}_2$  results the residual deviations appear consistent with effects produced by higher-order terms such as four-derivative contact interactions. For  $^1P_1$  and  $^3P_0$  there is some indication of higher-derivative effects for  $p_{\text{CM}}$  near 110 MeV.

The  $D$ -wave phase shifts are shown in Fig. 8 and 9. None of the  $D$ -wave data was used in the fitting of operator coefficients. For both  $\text{NLO}_1$  and  $\text{NLO}_2$  results the errors appear consistent with effects from higher-order interactions. The  $\text{NLO}_1$  deviations are somewhat smaller, though the  $\text{NLO}_1$  and  $\text{NLO}_2$  deviations appear similar in character. Overall the differences among  $\text{LO}_1$ ,  $\text{LO}_2$ ,  $\text{NLO}_1$ , and  $\text{NLO}_2$  results for the  $D$  waves are smaller than the corresponding differences for the  $S$  and  $P$  waves. This observation is consistent with the dominance of the one-pion exchange potential and validity of the Born approximation in higher partial waves.

The mixing parameter  $\varepsilon_1$  in the Stapp parameterization [41] is shown in Fig. 10. Results for  $\text{LO}_1$  and  $\text{NLO}_1$  are on the left, and results for  $\text{LO}_2$  and  $\text{NLO}_2$  are on the right. The pairs of points connected by dotted lines indicate pairs of solutions at  $k = k^I$  and  $k = k^{II}$  for the coupled  $^3S_1$ - $^3D_1$  channels. For  $\text{LO}_1$  it is interesting to note that  $\varepsilon_1$  has the wrong sign. For both  $\text{NLO}_1$  and  $\text{NLO}_2$  results the remaining deviations appear consistent with effects produced by higher-order interactions.

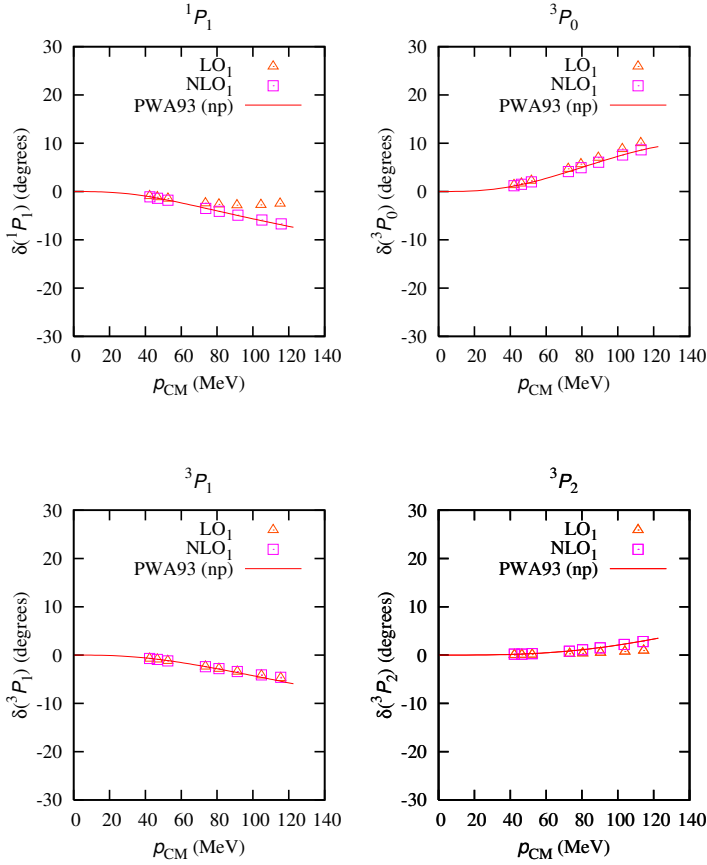


FIG. 6:  $P$ -wave phase shifts versus center-of-mass momentum for LO<sub>1</sub> and NLO<sub>1</sub>.

## VII. SUMMARY AND DISCUSSION

We have studied nucleon-nucleon scattering on the lattice at next-to-leading order in chiral effective field theory at momenta less than or equal to the pion mass. Throughout our analysis we tested model independence at fixed lattice spacing by repeating calculations using two different lattice actions. The first leading-order action LO<sub>1</sub> included instantaneous one-pion exchange and same-site contact interactions. The second leading-order action LO<sub>2</sub> included instantaneous one-pion exchange and Gaussian-smearred interactions. We computed next-to-leading-order corrections for these actions and in each case found results accurate up to corrections at higher order. In the second paper of this series we use the LO<sub>2</sub> and NLO<sub>2</sub> actions to compute the ground state of dilute neutron matter using Monte

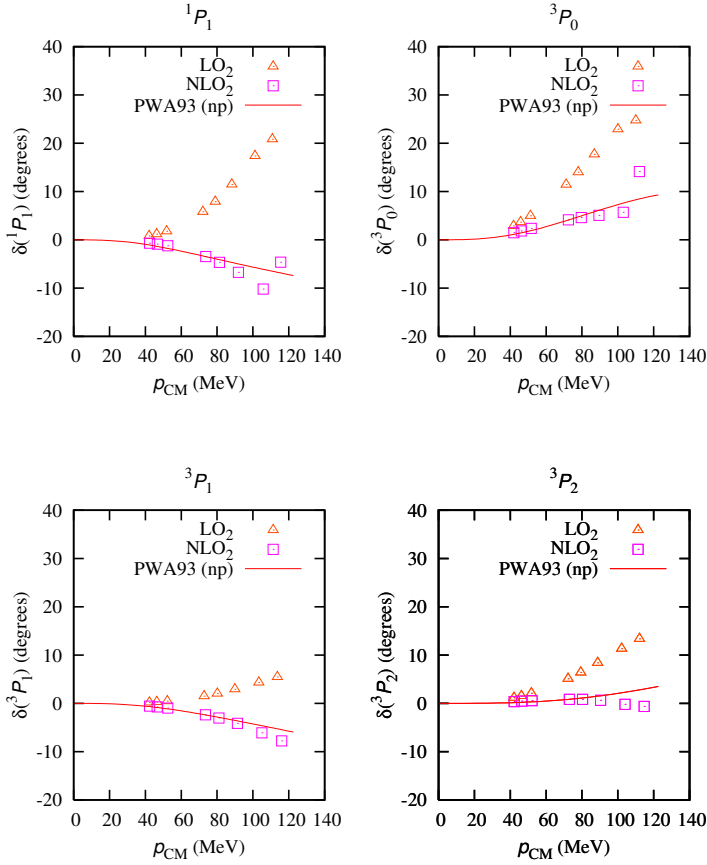


FIG. 7:  $P$ -wave phase shifts versus center-of-mass momentum for LO<sub>2</sub> and NLO<sub>2</sub>.

Carlo. This is done using the auxiliary-field transfer matrix method introduced in [13].

Overall we find that the Gaussian-smeared actions LO<sub>2</sub> and NLO<sub>2</sub> are more accurate than the standard actions LO<sub>1</sub> and NLO<sub>1</sub>. This can be seen most easily from the size of the required NLO corrections in Table II. For  $P$ -wave interactions, however, we see from comparing Fig. 6 and Fig. 7 that the standard actions LO<sub>1</sub> and NLO<sub>1</sub> are more accurate. In future studies it would be useful to try to find an improved LO action with accurate  $S$ -wave phase shifts and smaller  $P$ -wave attraction without inducing sign problems in Monte Carlo simulations.

The results presented here can be extended to higher orders in chiral effective field theory. If we continue with the low cutoff momentum  $\Lambda \approx 2.3m_\pi$ , then the NNLO two-pion exchange potential can be expanded in powers of  $q^2/(4m_\pi^2)$  in the same manner as the NLO two-pion

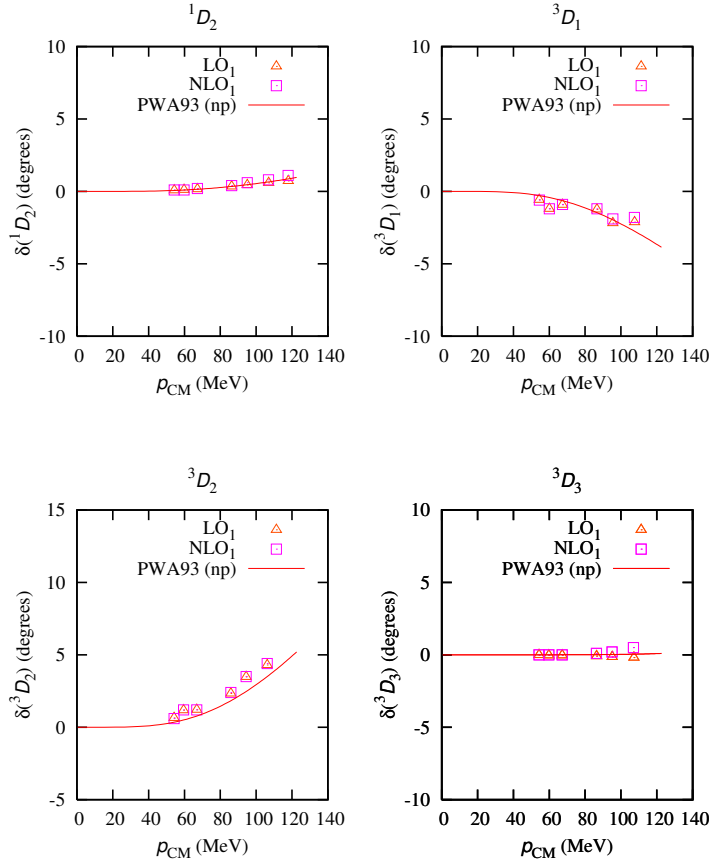


FIG. 8:  $D$ -wave phase shifts versus center-of-mass momentum for LO<sub>1</sub> and NLO<sub>1</sub>.

exchange potential. This expansion yields local operators which are either renormalizations of local operators with zero or two derivatives, local operators with four derivatives, or local operators with more than four derivatives. The operators with four derivatives should be treated in the same manner as local four-derivative operators appearing at N<sup>3</sup>LO in the usual chiral power counting.

In our analysis we have ignored small effects that appear in extraneous channels due to broken rotational invariance on the lattice. For example the mixed  $^3S_1$ - $^3D_1$  spherical waves each have some small admixture of an unphysical  $^3D_3$  component. In our analysis of  $\varepsilon_1$  we measured the ratio of  $^3S_1$  and  $^3D_1$  components and neglected this small  $^3D_3$  component. In the future we might prefer a more ambitious approach which explicitly removes the  $^3D_3$  component. This requires including local interactions which are invariant under the cubic

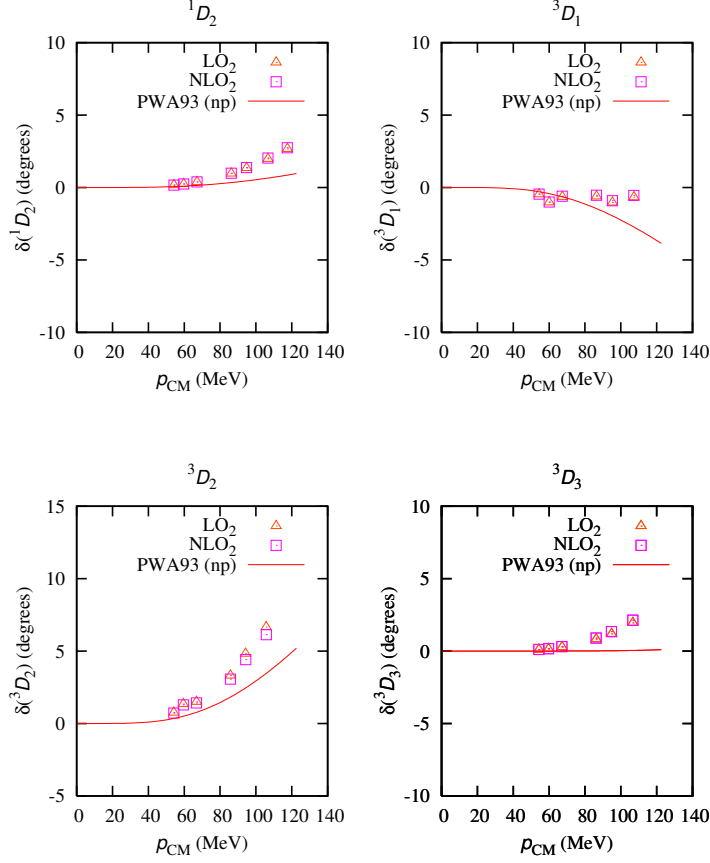


FIG. 9:  $D$ -wave phase shifts versus center-of-mass momentum for LO<sub>2</sub> and NLO<sub>2</sub>.

rotational group  $SO(3, \mathbb{Z})$  but not invariant under the full  $SO(3)$  symmetry. For example in addition to the  $SO(3)$ -invariant interaction

$$\frac{1}{2} : \sum_{\vec{n}} \sum_S \Delta_S \rho_S^{a^\dagger, a}(\vec{n}) \sum_{S'} \Delta_{S'} \rho_{S'}^{a^\dagger, a}(\vec{n}) :, \quad (80)$$

we should also include a small contribution from the  $SO(3, \mathbb{Z})$ -invariant but  $SO(3)$ -noninvariant operator

$$\frac{1}{2} : \sum_{\vec{n}} \sum_S \Delta_S \rho_S^{a^\dagger, a}(\vec{n}) \Delta_S \rho_S^{a^\dagger, a}(\vec{n}) :. \quad (81)$$



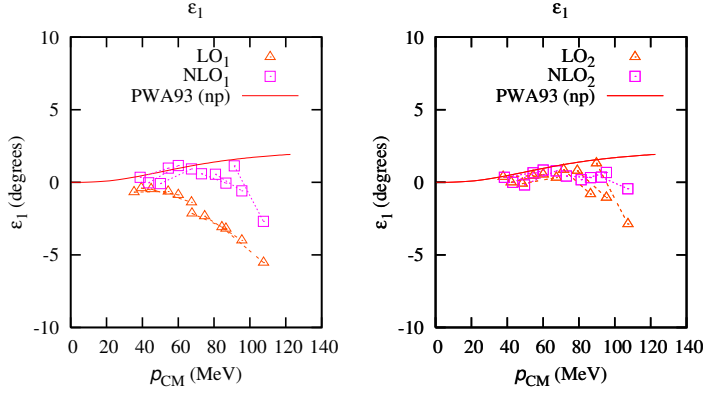


FIG. 10:  $\varepsilon_1$  mixing angle for  $LO_1$  and  $NLO_1$  on the left,  $LO_2$  and  $NLO_2$  on the right.

## Acknowledgements

Partial financial support from the Deutsche Forschungsgemeinschaft (SFB/TR 16), Helmholtz Association (contract number VH-NG-222 and VH-VI-231), and U.S. Department of Energy (DE-FG02-03ER41260) are gratefully acknowledged. This research is part of the EU Integrated Infrastructure Initiative in Hadron Physics under contract number RII3-CT-2004-506078. The computational resources for this project were provided by the John von Neumann Institute for Computing at the Forschungszentrum Jülich.

## APPENDIX A: CONTINUUM LIMIT OF THE NLO INTERACTIONS

### 1. One-nucleon matrix elements

The matrix elements of the local densities for single nucleon states are

$$\langle \vec{p}, i, j | \rho^{a^\dagger, a}(\vec{n}) | \vec{p}', i', j' \rangle = \delta_{ii'} \delta_{jj'} e^{i(\vec{p}' - \vec{p}) \cdot \vec{n}}, \quad (A1)$$

$$\langle \vec{p}, i, j | \rho_I^{a^\dagger, a}(\vec{n}) | \vec{p}', i', j' \rangle = \delta_{ii'} [\tau_I]_{jj'} e^{i(\vec{p}' - \vec{p}) \cdot \vec{n}}, \quad (A2)$$

$$\langle \vec{p}, i, j | \rho_S^{a^\dagger, a}(\vec{n}) | \vec{p}', i', j' \rangle = [\sigma_S]_{ii'} \delta_{jj'} e^{i(\vec{p}' - \vec{p}) \cdot \vec{n}}, \quad (A3)$$

$$\langle \vec{p}, i, j | \rho_{S,I}^{a^\dagger, a}(\vec{n}) | \vec{p}', i', j' \rangle = [\sigma_S]_{ii'} [\tau_I]_{jj'} e^{i(\vec{p}' - \vec{p}) \cdot \vec{n}}. \quad (A4)$$

The matrix elements for derivatives of these densities are found by taking  $f(\vec{n}) = e^{i(\vec{p}'-\vec{p})\cdot\vec{n}}$  and computing

$$\Delta_l f(\vec{n}) = e^{i(\vec{p}'-\vec{p})\cdot\vec{n}} \times \frac{1}{4} \sum_{\nu_1, \nu_2, \nu_3=0,1} (-1)^{\nu_1+1} e^{i(\vec{p}'-\vec{p})\cdot\vec{\nu}}, \quad (\text{A5})$$

$$\nabla_l^2 f(\vec{n}) = e^{i(\vec{p}'-\vec{p})\cdot\vec{n}} \times \left[ e^{i(\vec{p}'-\vec{p})\cdot\hat{l}} + e^{-i(\vec{p}'-\vec{p})\cdot\hat{l}} - 2 \right]. \quad (\text{A6})$$

In the continuum limit  $|\vec{p}'|$  and  $|\vec{p}|$  in units of inverse lattice spacing are small and so

$$\frac{1}{4} \sum_{\nu_1, \nu_2, \nu_3=0,1} (-1)^{\nu_1+1} e^{i(\vec{p}'-\vec{p})\cdot\vec{\nu}} \rightarrow i(p'_l - p_l), \quad (\text{A7})$$

$$e^{i(\vec{p}'-\vec{p})\cdot\hat{l}} + e^{-i(\vec{p}'-\vec{p})\cdot\hat{l}} - 2 \rightarrow -(p'_l - p_l)^2. \quad (\text{A8})$$

The matrix element for the SU(4)-invariant current density is

$$\langle \vec{p}, i, j | \Pi_l^{a^\dagger, a}(\vec{n}) | \vec{p}', i', j' \rangle = \delta_{ii'} \delta_{jj'} e^{i(\vec{p}'-\vec{p})\cdot\vec{n}} \times \frac{1}{4} \sum_{\nu_1, \nu_2, \nu_3=0,1} (-1)^{\nu_1+1} e^{i\vec{p}'\cdot\vec{\nu}} e^{-i\vec{p}\cdot\vec{\nu}(-l)}. \quad (\text{A9})$$

Similarly the matrix element for the spin current density is

$$\langle \vec{p}, i, j | \Pi_{l,S}^{a^\dagger, a}(\vec{n}) | \vec{p}', i', j' \rangle = [\sigma_S]_{ii'} \delta_{jj'} e^{i(\vec{p}'-\vec{p})\cdot\vec{n}} \times \frac{1}{4} \sum_{\nu_1, \nu_2, \nu_3=0,1} (-1)^{\nu_1+1} e^{i\vec{p}'\cdot\vec{\nu}} e^{-i\vec{p}\cdot\vec{\nu}(-l)}. \quad (\text{A10})$$

The other current densities are not needed for the NLO interactions. In the continuum limit

$$\frac{1}{4} \sum_{\nu_1, \nu_2, \nu_3=0,1} (-1)^{\nu_1+1} e^{i\vec{p}'\cdot\vec{\nu}} e^{-i\vec{p}\cdot\vec{\nu}(-l)} \rightarrow i(p'_l + p_l). \quad (\text{A11})$$

## 2. Two-nucleon matrix elements

The tree-level amplitude for two-nucleon scattering consists of contributions from direct and exchange diagrams. However for bookkeeping purposes we label the contact interactions according to the tree-level amplitude for scattering of two distinguishable nucleons. We imagine that one nucleon is of type  $A$  and the other nucleon is of type  $B$ . The interactions include densities and current densities for both  $A$  and  $B$ . For example the SU(4)-invariant density and current density become

$$\rho^{a^\dagger, a}(\vec{n}) \rightarrow \rho^{a^\dagger_A, a_A}(\vec{n}) + \rho^{a^\dagger_B, a_B}(\vec{n}), \quad (\text{A12})$$

$$\Pi_l^{a^\dagger, a}(\vec{n}) \rightarrow \Pi_l^{a^\dagger_A, a_A}(\vec{n}) + \Pi_l^{a^\dagger_B, a_B}(\vec{n}). \quad (\text{A13})$$

Let the incoming momenta be  $\vec{p}_i^A$  and  $\vec{p}_i^B$  and the outgoing momenta be  $\vec{p}_f^A$  and  $\vec{p}_f^B$ . The  $t$ -channel momentum transfer is

$$\vec{q} = \vec{p}_i^A - \vec{p}_f^A = -\vec{p}_i^B + \vec{p}_f^B, \quad (\text{A14})$$

and the  $u$ -channel exchanged momentum transfer is

$$\vec{k} = \vec{p}_i^A - \vec{p}_f^B = -\vec{p}_i^B + \vec{p}_f^A. \quad (\text{A15})$$

For these incoming and outgoing states the amplitudes for  $\Delta V^{(0)}$  are

$$\mathcal{A}(\Delta V) = \Delta C, \quad (\text{A16})$$

$$\mathcal{A}(\Delta V_{I^2}) = \Delta C_{I^2} \sum_I \tau_I^A \tau_I^B. \quad (\text{A17})$$

In the continuum limit the amplitudes for  $V^{(2)}$  are

$$\mathcal{A}(V_{q^2}) \rightarrow C_{q^2} q^2, \quad (\text{A18})$$

$$\mathcal{A}(V_{I^2, q^2}) \rightarrow C_{I^2, q^2} q^2 \sum_I \tau_I^A \tau_I^B, \quad (\text{A19})$$

$$\mathcal{A}(V_{S^2, q^2}) \rightarrow C_{S^2, q^2} q^2 \sum_S \sigma_S^A \sigma_S^B, \quad (\text{A20})$$

$$\mathcal{A}(V_{S^2, I^2, q^2}) \rightarrow C_{S^2, I^2, q^2} q^2 \sum_S \sigma_S^A \sigma_S^B \sum_I \tau_I^A \tau_I^B, \quad (\text{A21})$$

$$\mathcal{A}(V_{(q \cdot S)^2}) \rightarrow C_{(q \cdot S)^2} \sum_S q_S \sigma_S^A \sum_{S'} q_{S'} \sigma_{S'}^B, \quad (\text{A22})$$

$$\mathcal{A}(V_{I^2, (q \cdot S)^2}) \rightarrow C_{I^2, (q \cdot S)^2} \sum_I \tau_I^A \tau_I^B \sum_S q_S \sigma_S^A \sum_{S'} q_{S'} \sigma_{S'}^B, \quad (\text{A23})$$

$$\mathcal{A}(V_{(iq \times S) \cdot k}) \rightarrow i C_{(iq \times S) \cdot k} \sum_{l, S, l'} \varepsilon_{l S l'} q_l (\sigma^A + \sigma^B)_S k_{l'}. \quad (\text{A24})$$

Most of these are straightforward, however the spin-orbit amplitude  $\mathcal{A}(V_{(iq \times S) \cdot k})$  requires some derivation. In terms of the incoming and outgoing momenta,

$$\begin{aligned} & \mathcal{A}(V_{(iq \times S) \cdot k}) \\ & \rightarrow \frac{i}{2} C_{(iq \times S) \cdot k} \sum_{l, S, l'} \varepsilon_{l S l'} \left[ (p_i^A + p_f^A)_l \sigma_S^B (p_i^B - p_f^B)_{l'} + (p_i^B + p_f^B)_l \sigma_S^A (p_i^A - p_f^A)_{l'} \right] \\ & + \frac{i}{2} C_{(iq \times S) \cdot k} \sum_{l, S, l'} \varepsilon_{l S l'} \left[ (p_i^A + p_f^A)_l \sigma_S^A (p_i^B - p_f^B)_{l'} + (p_i^B + p_f^B)_l \sigma_S^B (p_i^A - p_f^A)_{l'} \right]. \end{aligned} \quad (\text{A25})$$

We note that

$$\begin{aligned} \sum_{l,S,l'} \varepsilon_{lS l'} (p_i^A + p_f^A)_l \sigma_S^B (p_i^B - p_f^B)_{l'} &= - \sum_{l,S,l'} \varepsilon_{lS l'} \left[ (p_i^A + p_f^A)_l \sigma_S^B (p_i^A - p_f^A)_{l'} \right] \\ &= - \sum_{l,S,l'} \varepsilon_{lS l'} \left[ (2p_i^A)_l \sigma_S^B (p_i^A - p_f^A)_{l'} \right]. \end{aligned} \quad (\text{A26})$$

Similarly

$$\sum_{l,S,l'} \varepsilon_{lS l'} (p_i^B + p_f^B)_l \sigma_S^A (p_i^A - p_f^A)_{l'} = - \sum_{l,S,l'} \varepsilon_{lS l'} \left[ (2p_f^B)_l \sigma_S^A (p_i^B - p_f^B)_{l'} \right], \quad (\text{A27})$$

$$\sum_{l,S,l'} \varepsilon_{lS l'} (p_i^A + p_f^A)_l \sigma_S^A (p_i^B - p_f^B)_{l'} = - \sum_{l,S,l'} \varepsilon_{lS l'} \left[ (2p_i^A)_l \sigma_S^A (p_i^A - p_f^A)_{l'} \right], \quad (\text{A28})$$

$$\sum_{l,S,l'} \varepsilon_{lS l'} (p_i^B + p_f^B)_l \sigma_S^B (p_i^A - p_f^A)_{l'} = - \sum_{l,S,l'} \varepsilon_{lS l'} \left[ (2p_f^B)_l \sigma_S^B (p_i^B - p_f^B)_{l'} \right]. \quad (\text{A29})$$

The sum of the four terms in Eq. (A26)-(A29) gives

$$\sum_{l,S,l'} \varepsilon_{lS l'} \left[ - (2p_i^A)_l \sigma_S^B q_{l'} + (2p_f^B)_l \sigma_S^A q_{l'} - (2p_i^A)_l \sigma_S^A q_{l'} + (2p_f^B)_l \sigma_S^B q_{l'} \right], \quad (\text{A30})$$

which equals

$$\sum_{l,S,l'} \varepsilon_{lS l'} \left[ -2k_l \sigma_S^B q_{l'} - 2k_l \sigma_S^A q_{l'} \right]. \quad (\text{A31})$$

We therefore find

$$\begin{aligned} \mathcal{A}(V_{(iq \times S) \cdot k}) &= -i C_{(iq \times S) \cdot k} \sum_{l,S,l'} \varepsilon_{lS l'} \left[ k_l \sigma_S^B q_{l'} + k_l \sigma_S^A q_{l'} \right] \\ &= i C_{(iq \times S) \cdot k} \sum_{l,S,l'} \varepsilon_{lS l'} q_l (\sigma^A + \sigma^B)_S k_{l'}. \end{aligned} \quad (\text{A32})$$

- 
- [1] H. M. Müller, S. E. Koonin, R. Seki, and U. van Kolck, Phys. Rev. **C61**, 044320 (2000), nucl-th/9910038.
- [2] T. Abe, R. Seki, and A. N. Kocharian, Phys. Rev. **C70**, 014315 (2004), erratum-ibid. C71 (2005) 059902, nucl-th/0312125.
- [3] S. Chandrasekharan, M. Pepe, F. D. Steffen, and U. J. Wiese, Nucl. Phys. Proc. Suppl. **129**, 507 (2004), hep-lat/0309093.
- [4] S. Chandrasekharan, M. Pepe, F. D. Steffen, and U. J. Wiese, JHEP **12**, 035 (2003), hep-lat/0306020.

- [5] D. Lee, B. Borasoy, and T. Schäfer, Phys. Rev. **C70**, 014007 (2004), nucl-th/0402072.
- [6] D. Lee and T. Schäfer, Phys. Rev. **C72**, 024006 (2005), nucl-th/0412002.
- [7] M. Hamilton, I. Lynch, and D. Lee, Phys. Rev. **C71**, 044005 (2005), nucl-th/0412014.
- [8] R. Seki and U. van Kolck, Phys. Rev. **C73**, 044006 (2006), nucl-th/0509094.
- [9] D. Lee and T. Schäfer, Phys. Rev. **C73**, 015201 (2006), nucl-th/0509017.
- [10] D. Lee and T. Schäfer, Phys. Rev. **C73**, 015202 (2006), nucl-th/0509018.
- [11] B. Borasoy, H. Krebs, D. Lee, and U.-G. Meißner, Nucl. Phys. **A768**, 179 (2006), nucl-th/0510047.
- [12] F. de Soto and J. Carbonell (2006), hep-lat/0610040.
- [13] B. Borasoy, E. Epelbaum, H. Krebs, D. Lee, and U.-G. Meißner, Eur. Phys. J. **A31**, 105 (2007), nucl-th/0611087.
- [14] D. Lee and R. Thomson, Phys. Rev. **C75**, 064003 (2007), nucl-th/0701048.
- [15] T. Abe and R. Seki (2007), arXiv:0708.2523 [nucl-th].
- [16] T. Abe and R. Seki (2007), arXiv:0708.2524 [nucl-th].
- [17] B. Borasoy, E. Epelbaum, H. Krebs, D. Lee, and U.-G. Meißner, Eur. Phys. J. **A34**, 185 (2007), arXiv:0708.1780 [nucl-th].
- [18] S. Weinberg, Phys. Lett. **B251**, 288 (1990).
- [19] S. Weinberg, Nucl. Phys. **B363**, 3 (1991).
- [20] C. Ordonez and U. van Kolck, Phys. Lett. **B291**, 459 (1992).
- [21] C. Ordonez, L. Ray, and U. van Kolck, Phys. Rev. Lett. **72**, 1982 (1994).
- [22] C. Ordonez, L. Ray, and U. van Kolck, Phys. Rev. **C53**, 2086 (1996), hep-ph/9511380.
- [23] E. Epelbaum, W. Glockle, and U.-G. Meißner, Nucl. Phys. **A637**, 107 (1998), nucl-th/9801064.
- [24] E. Epelbaum, W. Gloeckle, and U.-G. Meißner, Nucl. Phys. **A671**, 295 (2000), nucl-th/9910064.
- [25] J. L. Friar and S. A. Coon, Phys. Rev. **C49**, 1272 (1994).
- [26] N. Kaiser, R. Brockmann, and W. Weise, Nucl. Phys. **A625**, 758 (1997), nucl-th/9706045.
- [27] E. Y. Loh, J. E. Gubernatis, R. T. Scalettar, S. R. White, D. J. Scalapino, and R. L. Sugar, Phys. Rev. **B41**, 9301 (1990).
- [28] S. E. Koonin, D. J. Dean, and K. Langanke, Phys. Rept. **278**, 1 (1997).
- [29] J.-W. Chen, D. Lee, and T. Schäfer, Phys. Rev. Lett. **93**, 242302 (2004), nucl-th/0408043.
- [30] S. K. Bogner, T. T. S. Kuo, A. Schwenk, D. R. Entem, and R. Machleidt, Phys. Lett. **B576**,

- 265 (2003), nucl-th/0108041.
- [31] S. K. Bogner, T. T. S. Kuo, and A. Schwenk, Phys. Rept. **386**, 1 (2003), nucl-th/0305035.
  - [32] D. B. Kaplan, M. J. Savage, and M. B. Wise, Nucl. Phys. **B478**, 629 (1996), nucl-th/9605002.
  - [33] D. B. Kaplan, M. J. Savage, and M. B. Wise, Nucl. Phys. **B534**, 329 (1998), nucl-th/9802075.
  - [34] S. R. Beane, P. F. Bedaque, M. J. Savage, and U. van Kolck, Nucl. Phys. **A700**, 377 (2002), nucl-th/0104030.
  - [35] A. Nogga, R. G. E. Timmermans, and U. van Kolck, Phys. Rev. **C72**, 054006 (2005), nucl-th/0506005.
  - [36] M. C. Birse, Phys. Rev. **C74**, 014003 (2006), nucl-th/0507077.
  - [37] E. Epelbaum and U.-G. Meißner (2006), nucl-th/0609037.
  - [38] M. C. Birse, Phys. Rev. **C76**, 034002 (2007), arXiv:0706.0984 [nucl-th].
  - [39] E. Wigner, Phys. Rev. **51**, 106 (1937).
  - [40] V. G. J. Stoks, R. A. M. Kompl, M. C. M. Rentmeester, and J. J. de Swart, Phys. Rev. **C48**, 792 (1993).
  - [41] H. P. Stapp, T. J. Ypsilantis, and N. Metropolis, Phys. Rev. **105**, 302 (1957).